

NSLS-II Project

CONCEPTUAL DESIGN REPORT for the COHERENT SOFT X-RAY BEAMLINE AT NSLS-II



final draft Sep 2009

Intentionally blank.

Approvals and Reviewers

Compiled by

Cecilia Sánchez -Hanke, CSX Beamline Scientist, NSLS-II

Signature

Date

Approved

Qun Shen, XFD Director, NSLS-II

Reviewers

Stephen Kevan, BAT Spokesperson, on behalf of the BAT

Andy Broadbent, Beamlines Manager

Nicholas Gmür, ESH Coordinator, NSLS-II

Sushil Sharma, Mechanical Engineering Group Leader, NSLS-II

Document Updates

The Conceptual Design Report for the Coherent Soft X-ray Beamline at NSLS-II is a controlled document, revised under change control.

Version No.	Date	Changes made
1	30-Sep-09	final draft, submitted to BAT

Intentionally blank.

Contents

1	INTRODUCTION	1
1.1	INTRODUCTION.....	1
1.2	BEAMLINE REQUIREMENTS	1
1.3	BEAMLINE ADVISORY TEAM (BAT).....	3
1.4	REPRESENTATIVE EXPERIMENTS	3
2	BEAMLINE LAYOUT.....	4
2.1	OVERVIEW	4
2.2	INSERTION DEVICE AND LOW β STRAIGHT SECTION AND OPERATION MODES	5
2.3	FRONT END	7
2.4	OPTICAL LAYOUT.....	8
2.5	BEAMLINE PERFORMANCE AND RAY TRACING.....	12
2.7	X-RAY TRACING.....	20
3	END STATION INSTRUMENTATION	22
4	SPECIAL BEAMLINE REQUIREMENTS.....	24
5	REFERENCES	26
	APPENDIX 1: SCHEDULE.....	27
	APPENDIX 2: ADDITIONAL INFORMATION	29
	PREVIOUS FACILITY REPORTS	29
	TIMING REQUIREMENTS FOR ULTRAFAST EXPERIMENTS (BY D. ARENA).....	29
	ESTIMATES FOR DATA STORAGE AND DATA PROCESSING (BY D. SHAPIRO).....	30

Acronyms

ADP	Avalanche Photon Diode
Be	Beryllium
CCD	Charge Coupled Device
CDI	Coherent Diffraction Imaging
CMPMS	Condensed Matter Physics and Materials Science
DW	Damping Wiggler
FEA	Finite Element Analysis
HEG	High-Energy Grating
IVUV	In-Vacuum Undulator
LEG	Low-Energy Grating
LoI	Letter of Interest
MEG	Medium-Energy Grating
ML	Multilayers
OH	Optics Hutch
PGM-VLS	Planar Grating Monochromator – Variable Length spacing
SNR	Signal-to-Noise Ratio
UHV	Ultra High Vacuum
VIPIC	Vertically Integrating Pixel Imaging Chip
XBPM	X-ray Beam Position Monitors

1 INTRODUCTION

1.1 Introduction

This conceptual design report describes the optical design for the coherent soft x-ray NSLS-II project beamline at the ~85% completion level. The document will primarily describe optical design, including the optical layout and calculations that support the expected performance of the Coherent Soft X-ray (CSX) beamline. The ~85% completion level of the optical design refers to our intention to complete this design and achieve the 100% of completion and prepare the final design report after an in-depth beamline performance study has been completed. This study will include finite element analysis on the required optical components and a wavefront analysis of both branches of the CSX beamline. We expect to finish these studies and include them in the preliminary design report, targeted for completion one year from now.

“This document describes, in some detail, the conceptual design of the optical layout of the CSX NSLS-II project beamline. We describe a unique state-of-the-art optical design of a soft x-ray beamline with two branches, one optimized to deliver the highest possible spatially coherent flux and one optimised for the highest-performance polarization-sensitive experiments. The coherence branch maximizes flux by minimizing the number of optical reflections. The polarization experiments demand full control of the beam polarization, including the capability to switch between opposite polarization states at rates from 10 Hz to 1 kHz. The CSX beamline optical design addresses perfectly the experimental requirements for the CSX beamline, as recommended by the CSX Beamline Advisory Team (BAT), as stated in the letter of interest for this beamline ”

In the search of the best possible optical layout design, the CSX beamline team has developed a very active collaboration with the beamline BAT. The design presented in this document is the result of the combined efforts of staff from the NSLS-II Project eXperimental Facilities Division (XFD) and Accelerator Systems Division (ASD), the NSLS Experimental Systems Division, and the CSX beamline BAT. The CSX beamline team would like to thank S.L. Hulbert and R. Reininger to their contributions to the content of the document and all of the collaborators for their contribution to the CDR.

Disclaimer: This document contains content from the Coherent Soft X-ray Beamline Advisory Team Letter of Interest document, as well as from the previous NSLS-II Project conceptual design reports http://www.bnl.gov/nsls2/project/CDR/Ch_11_Experimental_Facilities.pdf and preliminary design report http://www.bnl.gov/nsls2/project/PDR/2-ExFac_Ch_004_CSX.PDF] both attached to the “additional information” APPENDIX . and from documents used to prepare all of the above.

Disclaimer: This document contains sections from the coherent soft x-ray beamline advisory team letter of interest (LoI) document, as well as from other documents used in the preparation of that document.

1.2 Beamline Requirements

This report compiles technical information regarding the optical layout of the CSX beamline. This soft x-ray beamline will operate in the 270 – 1700 eV energy range and will be optimized for “photon hungry” experiments such as experiments using coherence and experiments that are sensitive to the x-ray polarization. The proposed optical layout serves two technical goals, the first being the generation of a high flux of spatially coherent photons in one branch, and the second being the generation of high photon flux with high resolving power with full control of the x-ray polarization. The proposed design requires two insertion devices in order to provide simultaneously two photon beams with opposite polarizations (for example, left- and right-circular) for the polarization control branch and also be able to operate as a single device in order to maximize the coherent flux for the coherence branch. We propose that both of the insertion devices be 49mm-period elliptically polarized undulators (EPU49) of the APPLE-II type, with two operating modes. In one of the operating modes, the IDs are in-line and phased, delivering a single beam to the coherence branch. In a second mode of operation, the two EPUs are canted in the horizontal plane by 0.16 mrad and deliver two angularly distinct beams, either to (a) serve the polarization branch

simultaneously with two beams of different polarizations or (b) deliver a single beam each of the branches for simultaneous, shared operation of both branches.

The CAD drawing below shows a 3D rendering of the CSX beamline, with its two branches, one for coherence and one for polarization control.

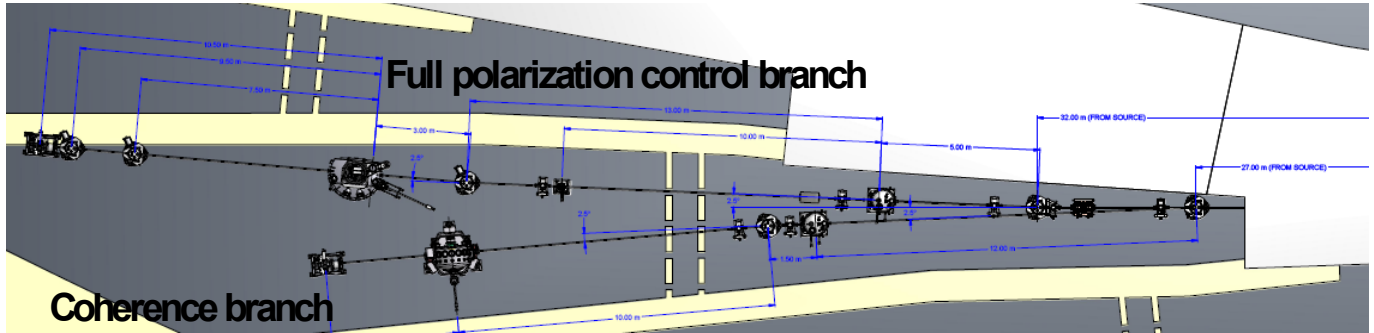


Figure 1 : Top view of CAD rendering of the CSX beamline (Courtesy Brian Mullany NSLS-II project)

The following is a list of additional requirements for the two CSX branches:

High coherent flux branch

- highest possible coherent flux
- variable focus position along the beam direction, by $\pm 0.5\text{m}$, to accommodate multiple experimental setups in the end-station, e.g. experiments using zone plates and those using pinholes-
- beam size on sample: $5\ \mu\text{m} \times 5\ \mu\text{m}$
- possibility to have a roll-up port
- beam stability (values)
- capability of source to provide circular (left or right) or linear (sigma or pi) polarization, slow switching

Polarization control branch

- highest possible photon flux
- modulated fast-switching polarization handedness, between circular left and right, or between linear sigma and pi, or other combinations, at rates from 10 Hz up to 1 kHz.
- smallest homogeneous beam size on the sample $5\ \mu\text{m} \times 5\ \mu\text{m}$
- 95% overlap on the sample of the beams from the two undulators
- minimization of the divergence between the photon beams from the two canted undulators.

1.3 Beamline Advisory Team (BAT)

In alphabetical order...

Prof. H. Ade

Department of Physics,
North Carolina State Univ., Raleigh, NC 27695-8202
Harald_Ade@ncsu.edu

Prof. Y. Idzerda

Department of physics
Montana State Univ., Bozeman, 59717-3840, MT
idzerda@physics.montana.edu

Dr. D. Arena

National Synchrotron Light Source,
Brookhaven National Laboratory, 11973 Upton NY
darena@bnl.gov

Prof. S. Kevan, BAT spokesperson

Department of physics,
Univ. of Oregon, Eugene OR,
kevan@physics.uoregon.edu

Dr. S. L. Hulbert,

National Synchrotron Light Source,
Brookhaven National Laboratory 11973 Upton NY
hulbert@bnl.gov

Dr. S. Wilkins

Condensed Matter Physics and Materials
Science department
Brookhaven National Laboratory, 11973 Upton NY
swilkins@bnl.gov,

1.4 Representative Experiments

The scope of the beamline has not change since the approval of this beamline LoI. The scientific case proposed in that document is still valid and the beamline optical design has been shaped to adapt to their technical requirements. The following text is an extract of the LoI document:

“A unifying theme of the motivation for the CSX beamline is to turn “photon hungry” coherent and polarization-sensitive experiments that are presently (2008) heroic, signal-limited experiments into high-throughput, high productivity techniques. For coherence experiments, this includes coherent diffraction (bulk and surface), phase retrieval imaging, soft x-ray photon correlation spectroscopy (XPCS), and coherent scattering. To date, these experiments have focused on the study of correlated electron systems but probably will evolve to other materials and systems, e.g. multi-ferroics. For polarization-sensitive experiments, the techniques include polarization-dependent spectroscopy, resonant scattering, time dependent and ultrafast dynamics of new materials and artificially engineered systems. Examples of these systems include highly dilute materials, micrometer-size single crystals, nanosized-materials, and interfaces. “

2 BEAMLINE LAYOUT

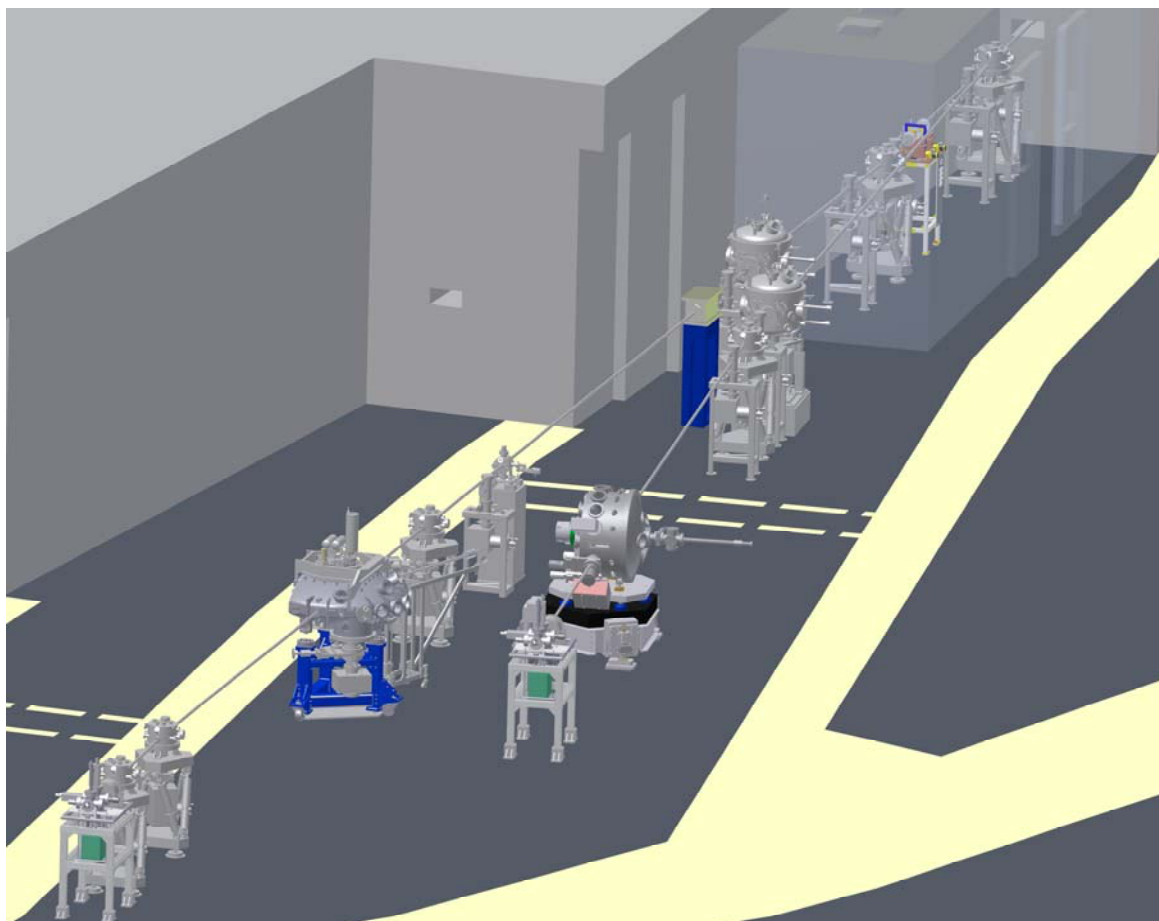


Figure 2: CAD 3D optical layout for the coherent soft x-ray beamline. (Courtesy Brian Mullany NSLS-II project)

2.1 Overview

Since the approval of the CSX beamline LoI (Sept. 2008), the scientific purpose of the beamline has not changed and the general beamline layout, consisting of two branches, one for coherence and one for polarization control, has persisted. The changes made to the beamline optical layout are a consequence of the adaptation of the beamline design to the refined experimental requirements of the beamline.

The general description of the CSX beamline, as presented originally in the CSX LoI document, is as follows:

“The CSX beamline consists of two branches, one dedicated to the generation and uses of the highest possible spatial coherence (CB) minimizing the number of reflections and optics in the beam path and the other dedicated to the highest-performance polarization-sensitive experiments (PB). Both branches need highly coherent flux and polarization control, which unifies them in the need for the longest possible elliptically-polarized undulator (EPU) source, i.e., the 2 x 2m-long EPU45s in a low-beta straight section. One branch (“Coherence”) sacrifices polarization switching rate somewhat in favor of highest possible coherent flux while the other (“Polarization”) sacrifices some coherent flux in favor of optimal polarization switching rate. Additionally, during times when the polarization switching rate does not need to be fast, each of the two 2m-long undulators could serve a separate branch, thereby providing 100% operational time for both branches with good brightness/flux and slow polarization switching rate.”

Changes to the CSX optical design

Since the approval of the CSX LoI, the period length of the proposed Elliptically Polarized Undulator (EPU) insertion devices has increased from 45 mm to 49 mm, as will be explained in the next section. In pursuing experimental flexibility and searching for the best possible beamline performance, the optical layout design presented in this document provides for a total of four experimental endstation locations, two for the Coherent branch (CB) and two for the Polarization branch (PB). The coherent branch optical design now provides an extended region of ± 2 meters along the beamline in the vicinity of the experimental endstation where the quality of the focused beam is almost identical, which can serve two experimental endstations without the need for an extra set of refocusing optics. In the Polarization Branch two experimental endstation positions have been provided, one optimized to have small horizontal angular divergence and a second one optimized for small spot on the sample.

2.2 Insertion Device and Low β Straight Section and Operation Modes

The insertion devices chosen for the CSX beamline, to provide elliptical, circular, and linear polarized soft x-rays are two 2 m long, 49 mm period Elliptically Polarized Undulators (EPU) of the APPLE-II type. This type of undulator is widely used in the soft x-ray community. Although earlier reports for the CSX beamline referred to an ID period length of 45 mm, the need to provide to the CSX user community with photon energies down to the Carbon K-edge (~ 270 eV) with linear polarization in both the horizontal and vertical directions, in addition to left- and right-hand circular polarization, required careful study to finalize this value. Figure 3 shows the results of calculations performed by O. Chubar (NSLS-II project, XFD and ASD) used to select the period length. The calculations indicate the minimum and maximum photon energies that can be achieved in the first harmonic with EPUs as a function of the period length assuming a minimum magnetic gap of 11.5 mm. Based on these results, the value of the ID period length was chosen to be 49 mm, which meets the state requirements for energy and polarization. Selecting a larger period length would enable access to lower photon energies at the price of reduced flux via reduced number of periods (in a fixed length). The panel on the right in Figure 3 shows that maximum usable photon energy from the fundamental of the EPU49 is 1700 eV.

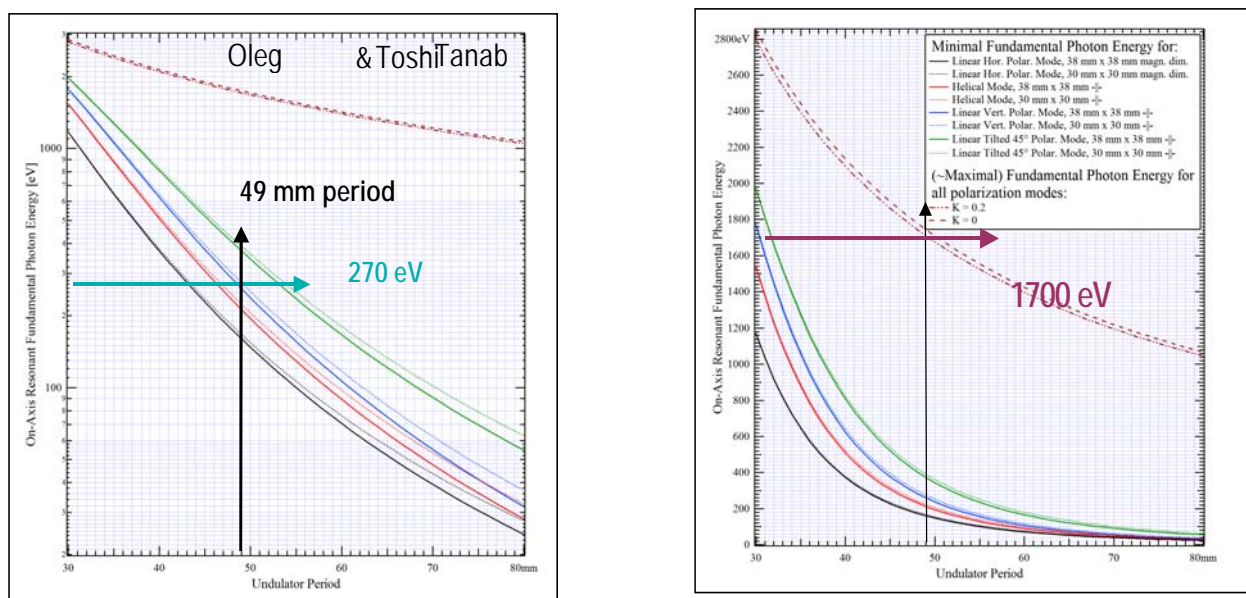


Figure 3 Calculated on-axis fundamental photon energy vs EPU period length. Left (right) panel y-axis scale is logarithmic (linear). Minimum fundamental photon energies for linear horizontal (black), circular (red), linear vertical (blue), and linear 45 degrees (green) polarizations are shown. The maximum usable fundamental photon energy is shown in brown. The 49 mm ID period length choice is marked, demonstrating that it can deliver photon energies down to 270 eV and up to 1700 eV in linear horizontal, vertical and circular polarizations. (Courtesy Oleg Chubar NSLS-II project)

ID operation modes

The CSX beamline is designed for three operation modes:

1. EPU's in-line and phased to function as one insertion device. This mode is used to deliver a single beam to the coherence branch.
2. EPU's horizontally canted by 0.16 mrad, each ID delivering a single photon beam to one branch (coherence and polarization).
3. EPU's horizontally canted by 0.16 mrad, delivering two photon beams of different or equal polarization to the polarization branch, to serve the fast polarization switching optical scheme which is described later.

Polarization control

The control of the source polarization for these Apple-II style EPU's is accomplished by mechanical adjustment of the phase of the horizontal undulator magnets with respect to the vertical ones, a process which lasts from ~ 1 sec to many seconds depending on the magnitude of the desired change in polarization. The technical specifications for the polarization branch require polarization switching rates from 10 Hz up to 1kHz, to reduce the signal-to-noise ratio and improve the sensitivity to smaller polarization sensitive signals. In the process of designing the optics layout two schemes were considered, both based on canted EPU's. In the first mode, the so-called static switching mode, the electron beam is shifted angularly through the insertion devices in order to deliver simultaneously two photon beams to the beamline that are separated by a fixed angular amount (0.16 mrad in the CSX case). In this mode, the polarization switching is accomplished by means of a mechanical chopper in the beamline, which alternately selects one of the two angularly-separated beams of opposite polarization. In the second mode, the dynamic switching mode, the electron beam is actively switched between the two IDs, delivering to the beamline one beam at a time with opposite polarization. The static mode requires a more complicated optical design, whereas the dynamic requires a more complicated accelerator design in the ID straight section. In addition, the dynamic mode requires fast switching of the electron beam itself, an operating mode which might lead to beam instabilities around the entire ring. And, furthermore, the simpler optical design connected with the dynamic switching mode will have poorer photon energy resolution than that of a system with optics keeping both undulators in focus. Finally, the static-switching beamline optical design presented below is in fact quite simple, consisting of only five optical elements in one branch (PB) and four in the other (CB). The decision of the CSX BAT was to adopt the static switching mode.

Phasing

The experiments to be performed at the coherent branch require as much coherent flux as possible. For that reason the soft x-ray science community is interested in being able to use both insertion devices, phased to operate as a single device. To make this operating mode possible, it is proposed to use an electromagnet located between the insertion devices to modulate the phase of the electron beam in the downstream ID to match the phase in the upstream ID. Wavefront propagation analysis will be performed to design the phasing magnet and simulate its effects on transverse coherence.

Straight section

The extremely low emittance of the electron beam in the low beta straight sections (the short straight sections) is essential to achieve the best performance of the CSX beamline. At the same time, the tiny photon beam size and angular divergence present a challenge for the mechanical design of the CSX beamline components (precision and accuracy of motions, vibration isolation, etc.). Similarly, high quality beam diagnostics are required in the ID straight section to ensure stable electron beam position and angle. The combined requirements of maximum undulator length, canting, phasing, and diagnostics could create a potential real estate problem for the layout of the CSX ID straight section. So far, this layout has been able to provide nearly all of the required

elements while preserving the desired 2 m length of the EPU49 undulators. Fig.4 is a CAD rendering of the current layout of the CSX ID straight section.

Quasiperiodicity

It is well known that higher undulator harmonics can be quite deleterious in all types of soft x-ray experiments, especially spectroscopy and scattering, and essentially impossible to remove experimentally. Various optical solutions have been implemented in soft x-ray beamlines, but always with compromises in flux and/or beam position. A much better solution is to shift the energy of the harmonics by an amount sufficient to move them out of the bandpass of the beamline monochromators. The commonly adopted solution is to introduce a small degree of quasi-periodicity to the undulator field profile. The only compromise in this solution is a 10-20% reduction in flux of the fundamental. A design study of the quasi-periodic EPU49 undulators for the CSX beamline will be undertaken in order to provide adequate harmonic rejection while minimizing the loss in flux from the fundamental.

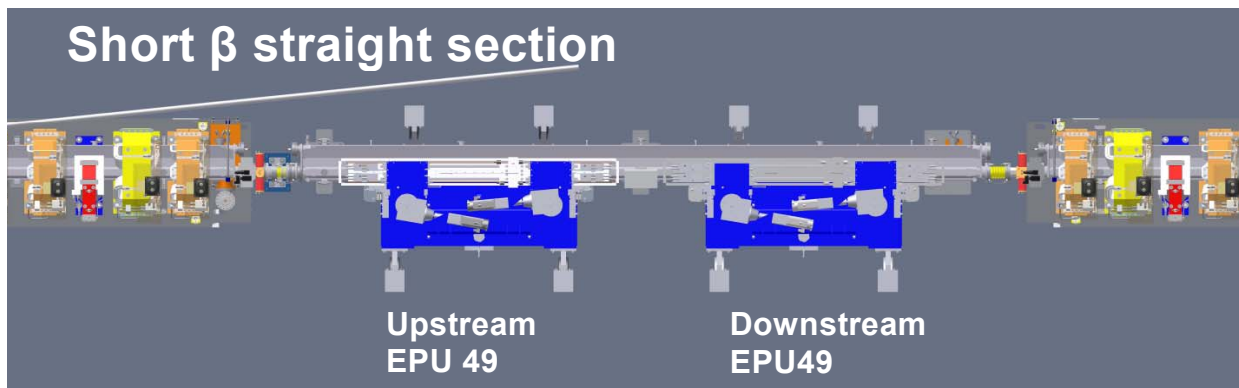


Figure 4: Layout of the CSX straight section, showing two 2m-long EPU49's, canting and phasing magnets, and beam position monitors. (Courtesy: R. Faussete, ASD, NSLS-II project)

2.3 Front End

The CSX soft x-ray beamline will operate windowless and under ultrahigh vacuum (UHV) conditions, 10^{-9} Torr or better, from the insertion device all the way downstream to the endstations. All beamline components will be UHV compatible, eliminating the need for differential pumping between the beamline and the front end.

Figure 5 shows the proposed standard front-end configuration showing the names of the standard elements. Note that the CSX front end is slightly different than the standard front-end model, in ways specific to the collimation and monitoring of soft x-rays. Additional instrumentation is included to aid CSX experimenters with the alignment and characterization of the soft x-ray beam during operations.

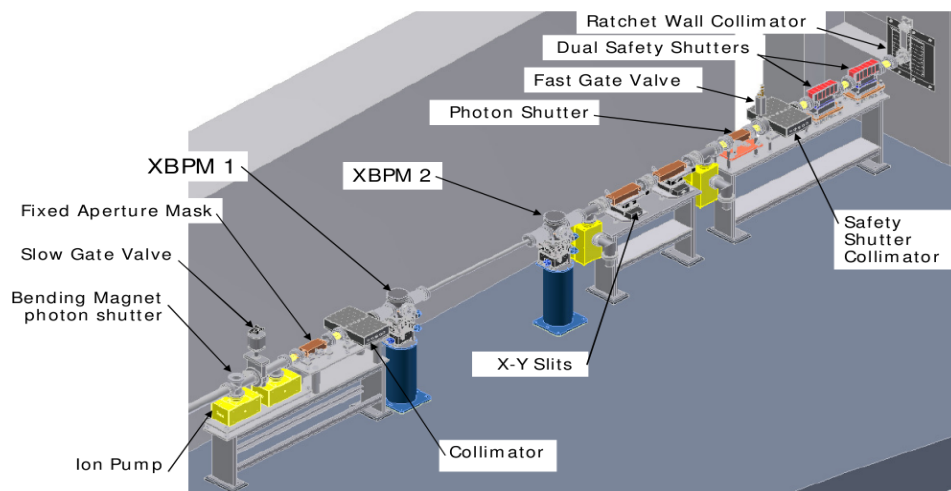


Figure 5 Proposed standard front-end configuration for the CSX project beamline. (Courtesy Lewis Doom Accelerator Systems Division, NSLS-II project).

Viewing along the beam direction from left to right, the front end components include: ion pump, photon shutter, slow gate valve, fixed aperture mask, collimator, X-ray Beam Position Monitor (XBPM) 1, XBPM 2, X-Y slits, photon shutter, safety shutter, collimator, fast gate valve, dual safety shutters, and ratchet wall collimator. The components that will be modified for the CSX front end, as compared to hard x-ray front ends, are: the fixed aperture mask, the XBPMs (1 and 2), and the X-Y slits.

The standard NSLS-II front end design will be utilized for the CSX beamline, with the following relatively minor changes: (a) the fixed aperture mask opening must be larger than the standard value, to match the maximum size of the two canted soft x-ray beams in the CSX canted undulator mode of operation, (b) it is desired to extract beam position signals from the X-Y slits, (c) the XBPMs must match the relatively soft photon energy and special polarizations of the CSX undulator beams.

Item (b) requires two engineering and design changes compared to the standard X-Y slit design: (i) the two L-shaped slit blades need to be replaced by four independent blades in order to extract separate horizontal and vertical beam position information, and (ii) each blade needs to be electrically isolated in order to sense beam position.

Item (c) requires special engineering and design of the CSX XBPMs in order to properly sense the relatively low photon energy EPU49 beams without wasting too many of them through absorption. Ideally, these XBPMs will not absorb any part of the beam that is needed at the sample positions in the endstations. The polarization sensitivity refers to the variation in beam shape for different polarization types (linear, circular, elliptical). These XBPMs also need to be able to independently sense the two angularly-separated undulator beams present in canted undulator mode. Such an XBPM has been designed at the Diamond Light Source, and may serve as a starting model for the NSLS-II dual-beam BPM.

2.4 Optical Layout

This section describes optical layout of the CSX beamline, including its major components. In addition to these major components, a number of other components will be needed. For example, instrumentation is needed for optical alignment and characterization of the photon beams, and later for efficient beamline operation. Conventional instrumentation will be needed for vacuum, interlocks, etc. A detailed design of these additional components will be initiated in the preliminary design phase.

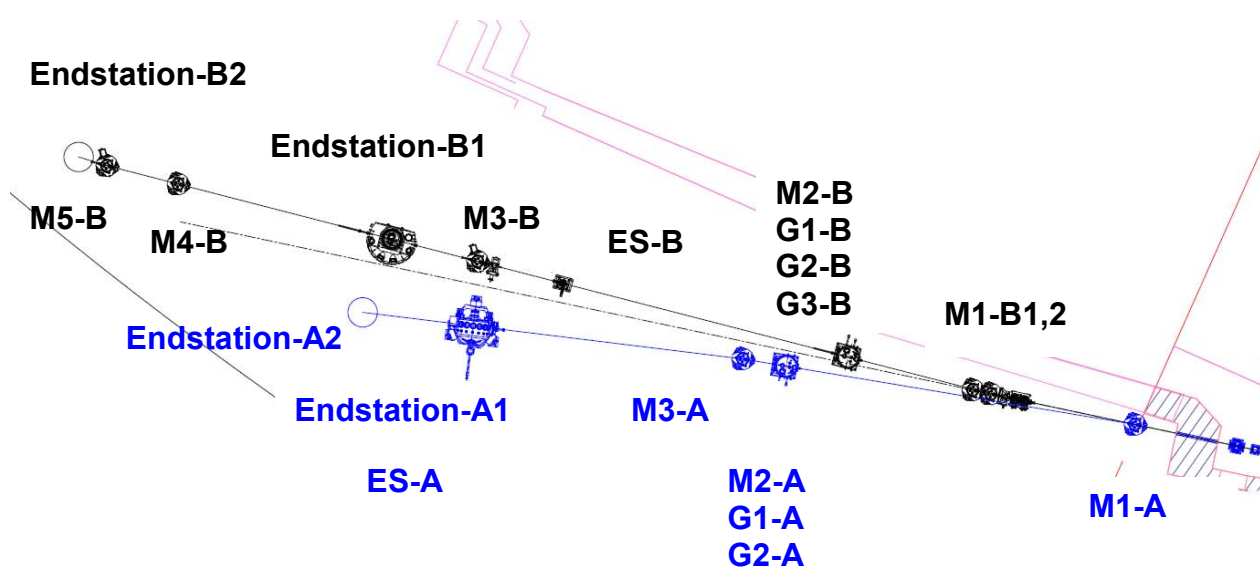


Figure 6: Top view CAD rendering of the optical layout of the CSX beamline optical layout. Major optical components are labeled.

Tables OL2 and OL3 list properties of the optical elements of the two branches of the CSX beamline, including: distance from the source, deflecting angle and direction, and the optical demagnification. In these tables, the optical components are designated as follows: M for mirrors, G for gratings, and ES for exit slits. The letters A and B are utilized to name the elements of the coherent (CB) and polarization (PB) branches, respectively. In the future and to achieve the 100% of the optical design more information will be provided such as the power dissipation or the required figure of merit.

Table 1: Optical Elements of the High Coherent Flux Branch.

Element name	Optical element	Distance (m) from source	Deflecting angle (degrees)	Direction of deflection	Demag., Hor./Ver
M1-A	Plane (water cooled)	27	88.75	Horizontal	
M2-A	Plane (water cooled)	38.7-38.9	84.5-88.6	Vertical	
	Gratings:	39	85.2-88.5	Vertical	
G1-A	LEG				/4.5-3.0
G2-A	MEG				/4.5-3.0
M3-A	Elliptical Cylinder (Bendable)	40.5	88.75	Horizontal	4.5-2.9/
ES-A	Exit Slit (sample position)	49.5 – 54.5			

A = Coherent branch item

ES = Exit Slits

G = Gratings

M = Mirrors

The numbers are the numerical order that that element appears in the optical layout design. In the future and to achieve the 100% of the optical design, more information will be provided, such as the power dissipation or the required figure of merit. Additionally, we envision having downstream of almost each of the mirror chambers (total of 7) diagnostic chambers with enough instrumentation to help in the alignment.

Table 2 : Optical Elements of the Full Polarization Control Branch.

Element name	Optical element	Distance (m) from straight center	Deflecting angle (degrees)	Direction of deflection	Demag. Hor./Ver
M1-B1 –	Toroidal (water cooled)	31.9	88.75	horizontal	1.5/collimating
M1-B2 –	Toroidal (water cooled)	32.1	88.75	horizontal	1.5/collimating
M2-B	Plane(water cooled)	36.6-36.91	85.4-88.8	Vertical	
	Gratings:	37	84.4-88.5	Vertical	
G1-B	LEG				/4.8
G2-B	MEG				/4.8
G3-B	HEG				/7
ES-B	Exit slit	47			
M3-B	Elliptical cylinder	50	88.75	Vertical	/1
	Sample B1	53			
M4-B	Elliptical cylinder	60.5	88.75	Vertical	/2.1
M5-B	Elliptical cylinder	62.5	88.75	horizontal	10/
	Sample B2	63.5			

B = Polarization branch item

ES = Exit Slits

G = Gratings

M = Mirrors

The numbers are the numerical order that that element appears in the optical layout design. In the future and to achieve the 100% of the optical design, more information will be provided, such as the power dissipation or the required figure of merit. Additionally, we envision having downstream of almost each of the mirror chambers (total of 7) diagnostic chambers with enough instrumentation to help in the alignment.

Not listed in tables 1 and 2 are the various beamline components that will complete the design of the beamline. These components include: (a) vacuum transport lines with vacuum components such as pumps, gauges, and hardware, (b) photon beam position monitors, (c) water-cooled white beam apertures with electrically isolated blades to dissipate the heat load and to define the external shape of the photon beams, (d) apertures for photon beam characterization, (e) diagnostic chambers containing fluorescence screens and grids for photon beam alignment and characterization, and (f) diagnostics chambers that will be used during operations to check the quality and the properties of the photon beams. In category (f) we will include instrumentation needed to characterize the degree of coherence and the degree of polarization. The designs of the diagnostics chambers will depend on the type of diagnostic and on location along the beamline.

The following is a functional listing of the major CSX beamline optical components, for both branches. Starting at the ratchet wall, the major components of the beamline are as follows:

White beam aperture The first element after the ratchet wall. This aperture will roughly define the size and shape of the beam and will also absorb unwanted portions of the EPU49 beams, mostly from very high harmonics

High coherent flux branch Branch designed to maximize coherent flux by minimizing the number of reflections

M1-A Planar, internally water-cooled mirror. Its function is to absorb power from unwanted high undulator harmonics, via appropriate choice of grazing angle, and thereby reduce the heat load on downstream optics. Also directs the photon beam into the coherent branch.

Monochromator A Variable line spacing plane grating monochromator

Plane mirror M2-A	Planar, internally water-cooled mirror, used to provide the proper angle of incidence on the grating
Grating Gn-A	Planar, side-cooled, variable line spacing diffraction grating, used both to disperse the incident pink beam and to focus it vertically at the exit slit. Two choices of grating are planned: G1-A (Low energy grating – LEG) and G2-A (medium energy grating - MEG).
M3-A	Horizontally deflecting and focusing bendable elliptical cylinder mirror. Focuses at the exit slit/pinhole/sample position.
Exit slit/pinhole A	slit/pinhole located at the beam focal point, to select photon energy and resolution as well as to define the degree of transverse spatial coherence. This slit/pinhole can be placed anywhere in an approx. 4m-long focal range of the beamline, due to the flexibility of the monochromators and the M3-A mirror.
Endstations A	The optical layout at this branch permits flexible location of more than one endstation along the beamline, over an approx. 4m-long focal range. Each endstation will need to provide its own exit slit/pinhole.
Polarization control branch	Branch designed to provide fast switching capability between photon beams with different polarizations
M1-B(1,2)	Two internally water-cooled horizontally deflecting and focusing toroidal mirrors. The minor radii are designed to collimate the beams ensuring that both beams are (vertically) focused at the exit slit by the monochromator. The major radii are slightly different from each other and are chosen to focus both beams at the sample position.
Monochromator B	Variable line spacing plane grating monochromators
Plane mirror M2-B	Planar, internally water-cooled mirror, used to provide the proper angle of incidence on the grating
Grating Gn-B	Planar, side-cooled, variable line spacing diffraction grating, used both to disperse the incident pink beam and to focus it vertically at the exit slit. Three choices of grating are planned: G1-B (Low energy grating – LEG), G2-B (medium energy grating - MEG), and G3-B (high energy grating - HEG)
Exit slit B	Vertically adjustable slit located at the beam focal point, to select photon energy and resolution. 10 μm will be the canonical vertical size, but will be variable from 5 μm to “infinity”
M3-B	Vertically focusing elliptical cylinder mirror (uncooled). Focuses the beam vertically onto the sample.
Endstation B1	Endstation location for small beam divergence.
M4-B	Vertically focusing elliptical cylinder mirror (uncooled). Refocuses the beam from endstation B1 vertically onto the sample in endstation B2.
M5-B	Horizontally focusing elliptical cylinder mirror (uncooled). Refocuses and demagnifies the beam from endstation B1 vertically onto the sample in endstation B2

Endstation B2

Endstation location for small beam spot.

It is planned that all the mirrors along both branches of the CSX beamline are supported with hexapod mounts. If possible and if the distance between the M-1B(1,2) mirrors allows it, each of these mirrors will be supported by its own hexapod.

Additionally, we envision the inclusion of diagnostic chambers to characterize the photon beams at various points along the beamline. The diagnostic instrumentation is especially useful for alignment, but will be used routinely during operation to verify beamline performance.

2.5 Beamline performance and ray tracing

The first priority for the CSX team was to converge to an optical layout to fulfill the beamline technical requirements to allow to perform as many as possible experiments proposed by the BAT in the CSX beamline LoI. The design of the beamline optics has evolved since the first proposed optical layout to the one proposed in this document. In the process of finalizing the optical, each change and variation was supported by ray tracing that will ensure that the optics keep performing in the scope of the beamline technical requirements, finite element analysis to ensure that the cooling for the first beamline optics is adequate to preserve the optics best performance and wave front analysis to ensure the efficient use of the sources.

High coherent flux branch

The suggested design for the coherence branch does not have an entrance slit, has four optical elements, and similar horizontal and vertical magnifications at the exit slit. The design and its expected performance are described in detail below.

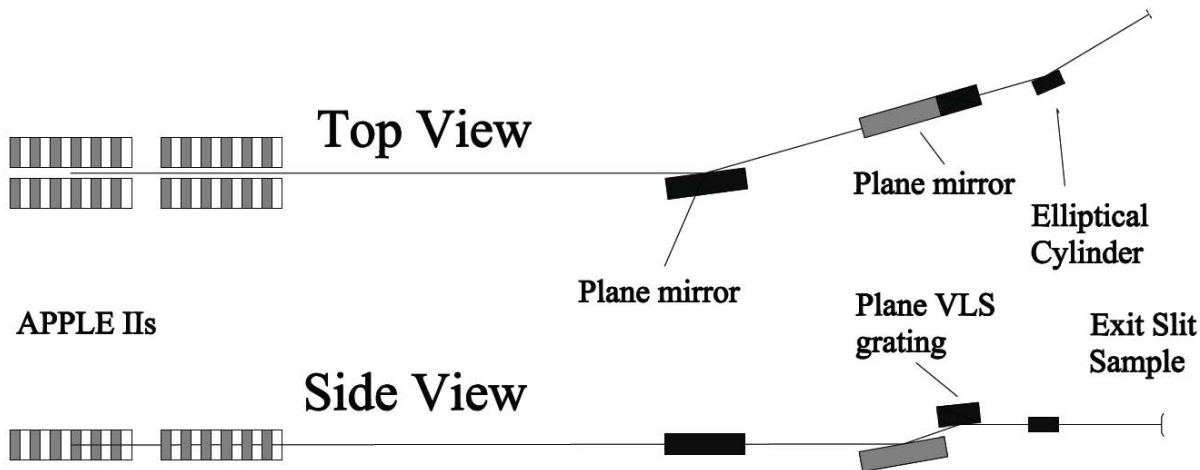


Figure 7: Top and side view of the coherence branch optics layout

Optical design

The parameters of the optical components are listed in Table 1 and a schematic layout showing the floor plan of the FPC is seen in Fig. 7

The first optical element, M1-A, is a plane mirror located outside the shield wall which deflects the beam horizontally by 2.5° . Its main function is to absorb the high photon energies emitted by the insertion device beyond the beamline range. Its angle of incidence and that of M3-A (see below) were chosen to have a reasonable horizontal separation between the full polarization control and the coherence branch.

The second optical element is a plane mirror, M2-A, which deflects the beam upwards (in the dispersion plane) towards the grating. This mirror needs to be rotated and translated in order to provide the grating with the correct angle of (normal) incidence, α , that will keep the defocus term of the grating zero at all wavelengths. The rotation and translation are actually incorporated in a simple rotation around an axis not on the mirror surface [1]. The angle of incidence on this mirror is given by $\gamma=0.5(\alpha-\beta)$, where β is the diffraction angle (negative).

The large distance between the source and the grating and the fact that the source is almost diffraction limited along the vertical direction means that a modest “resolving power” can only be achieved with a low line density grating and using a low c ($\cos \alpha/\cos \beta$) factor. To achieve the required “resolving power” of ≈ 2000 we chose two gratings with central line densities of 50 l/mm (LEG) and 100 l/mm (HEG) operating with $c = 1.1$. As mentioned above, the source will be either one or two IDs. The fact that the beamline does not have an entrance slit means that the resolving power will depend on the source in use. Furthermore, the vertical source position will vary depending on which source is used. This can be corrected by adjusting the c value. From the geometry and the chosen c value one obtains a magnification along the dispersion direction equal to 0.42 and 0.44 with two IDs and one ID, respectively.

The last element of the beamline (M3-A) is a bendable elliptical cylinder deflecting the beam horizontally by 2.5° and focusing it horizontally at the exit slit. We have chosen a bendable mirror to correct for the heat load induced slope error on the plane mirror as described in Ref.2 Its magnification is slightly lower than that of the monochromator, 0.42 with one ID and 0.41 with both IDs.

Resolving Power

The monochromator resolving power was calculated from the vector sum of all the relevant contributions to the resolution: source size, aberrations, slope errors, and exit slit.

The zeroing of the coma and spherical aberrations at 500 eV (1000 eV) for the LEG (HEG) with the quadratic and cubic term of the grating line density makes their contribution to the resolution negligible as compared to that of the source size. Meridional slope errors of $0.1 \mu\text{rad}$ in the plane elements and $0.5 \mu\text{rad}$ in the elliptical cylinder were assumed in the calculations. Their combined contribution to the resolution is comparable to that of the source size when one ID is used for photon energies ≥ 1000 eV, and better than the source when two IDs are used.

The exit slit width was set such that its contribution to the resolution is the same as that due to the source size. The required exit slit width is shown in Fig.8 as a function of the photon energy as well as the RMS divergence of the coherent flux for one and two IDs. Since the horizontal and vertical demagnification of the beamline are practically the same and the exit slit width was set for the same resolution as the coherent source, the horizontal aperture could be set to the same value.

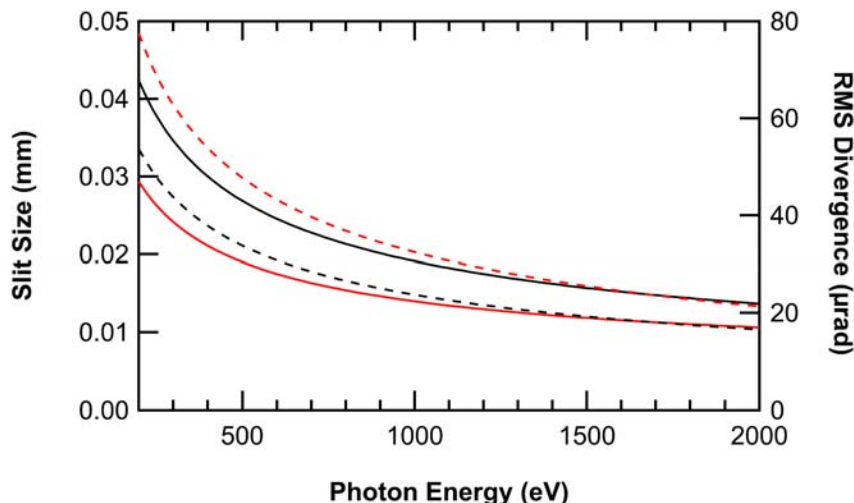


Figure 8. Left axis - Solid lines: Exit slit size yielding the same resolution as the source. Right Axes - Dashed lines: RMS divergence of the coherent flux. Red line: One ID; Black line two IDs
 The total “resolving power” calculated as explained above for one and two IDs with the LEG and HEG are shown in Fig. 9. As expected, the “RP” of the two IDs is worst that that of a single ID since the coherent source size is proportional to the square root of the device length.

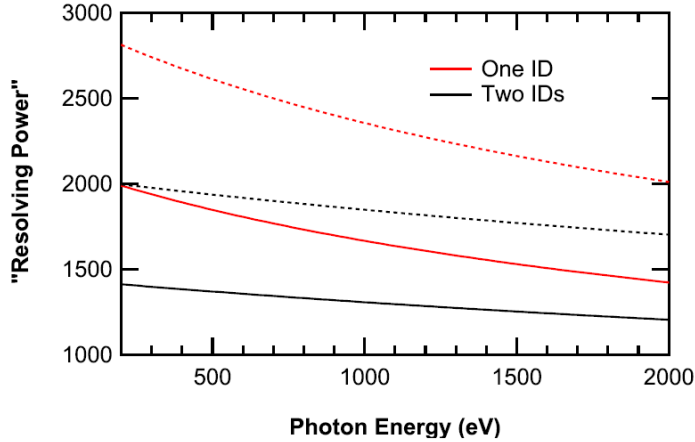


Figure 9: Total “RP”. Black traces: Two IDs; Red traces: One ID. Solid lines: LEG; Dashed lines: HEG.

We ray traced the beamline for several photon energies, with sources simulating one and two IDs, and with and without slope errors on the optical elements. Two representative examples confirming the analytical calculations are described below. Evidently, the contribution of the exit slit is not included in the ray tracings and therefore are quoted as resolving power.

The spot pattern at the exit slit plane showing a RP better than 2500 when one ID and the LEG are used and the monochromator is tuned to 250 eV is seen in Fig.10. The ray tracings include the same slope errors used in the analytical calculations. Without slope errors the RMS size in the dispersion direction is 9.9 μm , only slightly smaller than the one shown in Fig. 10. Along the horizontal direction the RMS size without the slope errors is 18 μm whereas those seen in the figure are 23 μm , the value expected when one takes into account the RMS slope error on M3-A.

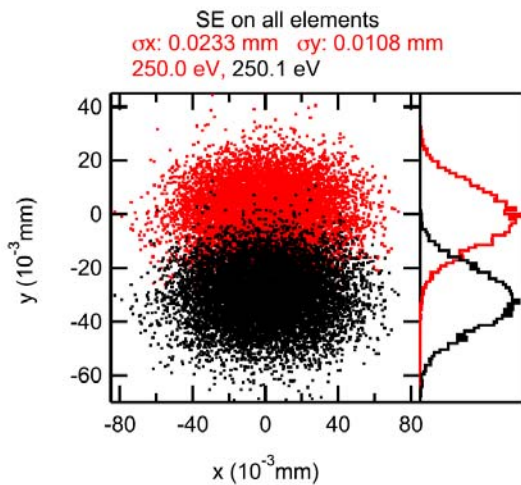


Figure 10: Spot pattern at the exit slit plane including slope errors on all optical elements. The RMS values shown above the figure are for 250 eV

The ray tracings results demonstrating a RP of ≈ 2000 when the upstream ID and the monochromator are tuned to 1500 eV are shown in Fig. 11. The RMS sizes without slope errors are 16 μm horizontally and 4.4 μm vertically. Since the last value is almost $\sqrt{2}$ smaller than the one in the figure means that the contribution due to the slope errors to the RP is comparable to that of the source.

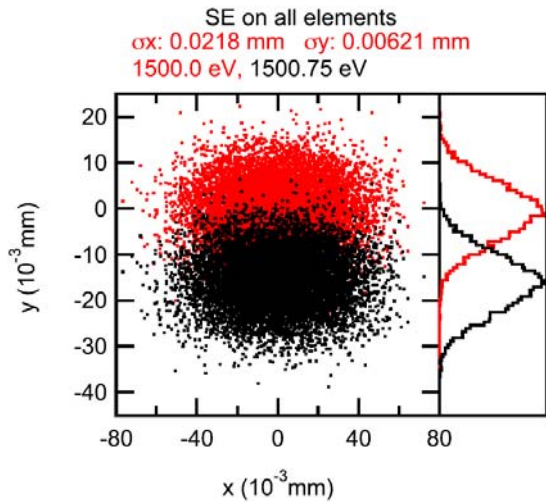


Figure 11: Spot pattern at the exit slit plane including slope errors on all optical elements. The RMS values shown above the figure are for 1500 eV

Coherence Flux

The calculated optical efficiency of the beamline including the mirrors reflectivities and the gratings efficiencies are shown in Fig.12. The gratings efficiencies were calculated using the exact electromagnetic theory [3] assuming they are blazed at an angle of 0.1° and the optical coating is Au on all elements. As seen in the figure, the optical efficiency using two gratings is higher than 10% between 200 and 1660 eV. The other traces in the figure represent the total beamline efficiency (ϵ). They include, in addition to the optical efficiency, the bandwidth correction due to the exit slit resolution (same as that of the source) as well as the factor due to the increase in the horizontal spot size due to the meridional slope errors on the elliptical cylinder (M3-A). The latter factor is 0.79 at 250 eV and decreases monotonically to 0.74 (0.65) when one (two) ID is used. The total efficiencies presented in Fig.12 will be used to calculate the coherent flux. We note in passing that the reduction in coherent flux due to the meridional slope errors on M2-A and the grating are taken into account through the "resolving power".

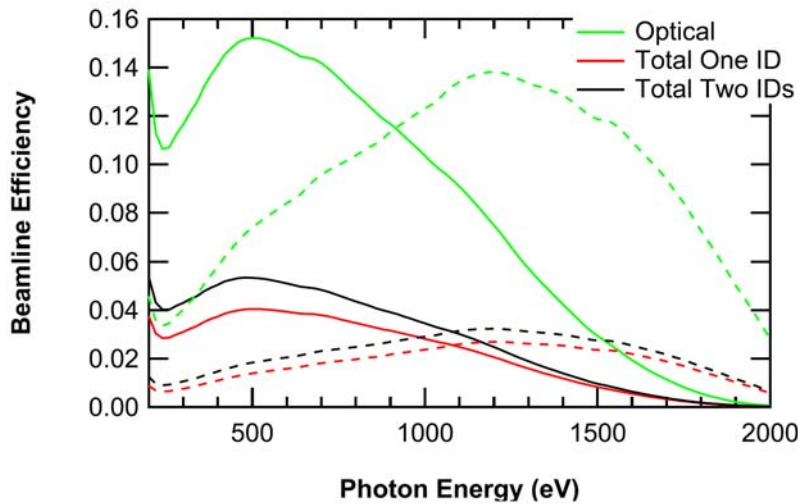


Figure 12: Green traces: Beamline optical efficiency. Red (Black) traces: Total efficiency when the source is one (two) ID. Solid lines: LEG; Dashed lines: HEG. See text.

The coherent flux transmitted by the beamline (F) for each one of the "RP" curves shown in Fig. 9 was calculated using $F = \epsilon B \lambda^2/4$, where B is the source brightness (calculated using the spectra code) [4] and λ is the wavelength.

The results shown on the figure make clear the need for a second grating to significantly increase the coherent flux for photon energies higher than 1.1 keV. With the two gratings and with two IDs the expected coherent flux delivered by the beamline will be higher than 3×10^{12} photons/s up to 1.6 keV at a “RP” better than 1300. With one ID the coherent flux will be $\geq 1 \times 10^{12}$ photons/s up to 1.7 keV at a “RP” better than 2000.

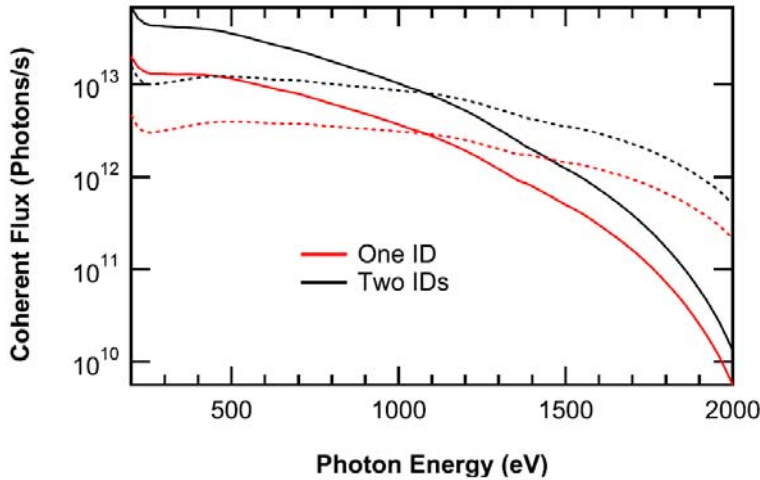


Figure 13: Coherence flux through the exit slit when using either one or two IDs.

Full polarization control branch

The description of the performance of the full polarization control branch was extracted mainly from a report/paper submitted for publication {ref RR}. The paper describes the optical design of the full polarization branch.

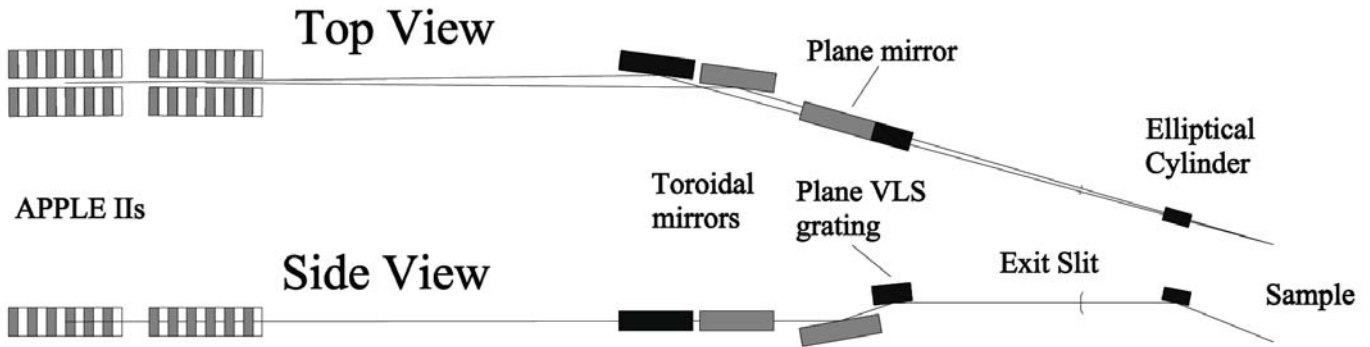


Figure 14: Schematic drawing of the full polarization control branch beamline optics

Optical design

Fig 14 shows the schematic drawing of the FPC branch optical layout. The distance from the source, the angles of incidence, the deflection of the optical elements, their demagnification, and the desired slope errors are listed in Table 2. The table also list the parameters of the Kirkpatrick-Baez (KB) pair (not shown in the figure) to be located downstream of the sample position and will be used to achieve a few-micron spot size for an additional experimental endstation or roll-up port to be located downstream of the scattering endstation [section 3 in this document].

The first two optical elements are a pair of internally water cooled toroidal mirrors deflecting the beam by $\approx 2.5^\circ$ in the horizontal plane. The upstream (downstream) mirror collects the beam from the upstream (downstream) ID. Since the vertical beams waists are separated by almost 2.5 m, the sagittal radii of the toroids are designed to

collimate the photon beams along the vertical direction. This arrangement was chosen in order to have both beams focused at the exit slit of the vertically dispersing monochromator. The meridional radii of the toroids are designed to focus the source horizontally at the sample position with approximately 1.5:1 demagnification. The next optical element is a plane mirror that illuminates a variable line spacing (VLS) plane grating [5-7]. The linear coefficient term in the line spacing variation function allows focusing of one chosen wavelength, while the quadratic term corrects the coma aberration, also at one wavelength. The important point of this optical design is the fact that with the plane mirror in front of the monochromator one can focus all wavelengths in the range covered by the grating by choosing the angle of incidence on this mirror such that the reflected ray illuminates the grating at the required angle of incidence. Since the angle of incidence on the plane mirror for a given VLS grating is determined by the focusing condition and the grating equation at that energy, it is advantageous to have at least three gratings that allow trading off resolution for flux while maintaining a fixed exit slit width. The chosen gratings have central line densities of 150 (Low Energy Grating, LEG), 400 (Medium Energy Grating, MEG), and 1200 (High Energy Grating, HEG) 1/mm. The LEG and MEG are operated with a c value ($c = \cos\beta / \cos\alpha$) of ≈ 1.5 whereas the HEG operates with $c \approx 2.2$ to allow for higher resolution [8].

An elliptical cylinder mirror (M3) downstream the exit slit deflects the beam downward by 2.5° , re-imaging the vertical exit slit onto the sample position in a 1:1 configuration. The focal spot at the sample position in the upstream experimental endstation is reimaged onto the sample position in the second endstation by a KB mirror pair consisting of elliptical cylinders. The first element of the pair deflects the beam upward by 2.5° and focuses along the vertical direction while the second deflects by the same angle in the horizontal plane and strongly demagnifies along this direction.

The beamline was ray traced using the SHADOW code [9] for several photon energies. Actually, two ray tracings were performed at each photon energy to take into account the fact that there are two sources and two different toroidal mirrors, one mirror for each source. The source files were generated with a separate code to take into account the fact that the vertical and horizontal source waists are separated by almost 1.25 m. The source parameters were assumed to be Gaussian with RMS values obtained as in Eq. 1 [10]

$$\Sigma_{x,y} = \sqrt{\sigma_{x,y}^2 + \frac{\lambda L}{2\pi^2}} \quad \text{and} \quad \Sigma'_{x,y} = \sqrt{\sigma_{x,y}^2 + \frac{\lambda}{2L}}, \quad (1)$$

where λ is the wavelength and L is the undulator length.

The figure errors in all the ray tracings were incorporated with SHADOW's PRESURFACE routine using a measured mirror profile scaled such as to obtain the meridional RMS slope errors specified in Table 2.

Fig 15a) shows the ray tracings of both beams at the exit slit plane of the monochromator for a photon energy of 300 eV when using the LEG. As seen in the figure, the two beams have only a small overlap. The vertical collimation means that both beams are in focus vertically at the exit slit. However, they differ in vertical focal spot size by approximately 10% owing to the 2.5m longitudinal separations of the two undulator sources.

The two beams at the sample position of the upstream experimental station when using a 10 μm exit slit opening and for 300 eV photons are displayed in Fig. 15b. For clarity, the two spot patterns have been separated in the figure. Their horizontal and vertical sizes are very close, but not identical. The difference is due to the different figure errors on the area of M3 that each beam illuminates. Nevertheless, the areas of the two spot patterns differ by less than 2%. The divergences of the two beams at the sample position in the upstream endstation are shown in Fig. 15c). Clearly, there is a larger divergence for both beams along the vertical direction compared to the horizontal direction owing to the higher vertical demagnification (see Table 2). The smaller horizontal divergence fulfills the experimental requirement of a small horizontal angular separation between the two beams.

As mentioned, the beamline will have a second branch for roll-up experiments requiring a small spot size. At this station, a spot size with a 5 μm diameter will be achieved, the beam divergences will be 1 mrad in both directions, and the horizontal angular separation between the beams will be 1.6 mrad.

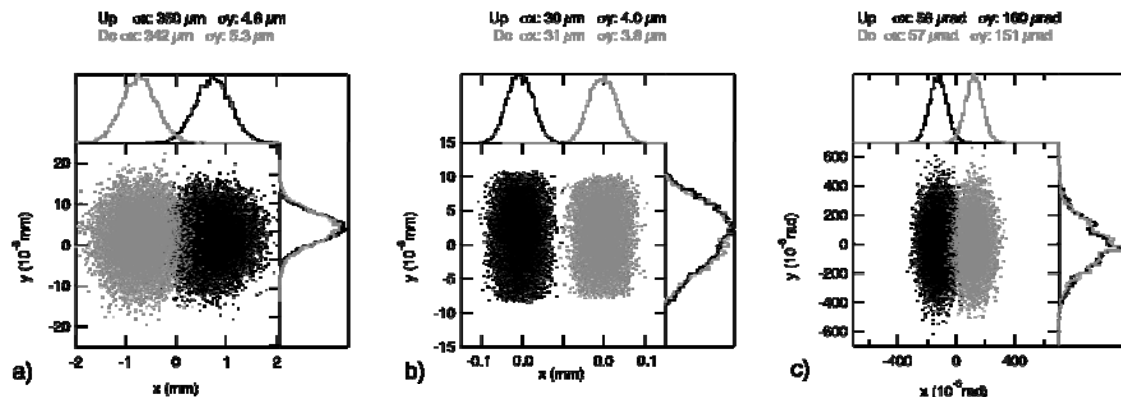


Figure 15. Ray tracings of beams from both undulators. a) At the exit slit plane; b) At the upstream endstation sample position; c) Beam divergences at the upstream endstation sample position. Photon energy 300 eV using the LEG.

Energy resolution

The expected monochromator resolution was calculated assuming the vertical spot size obtained using Eq.1, the slope errors specified in Table 2, and an exit slit width of 10 μm . All the other contributions, including coma, slope errors of the toroids, and higher order aberrations, are negligible in this design.

Fig. 16a summarizes the expected resolution of the monochromator for the three gratings when the exit slit opening is set to 10 μm . For the LEG and the MEG, the resolution term due to the source size is the largest at low photon energies whereas at higher photon energies the dominant term is that due to the exit slit. For the HEG, the largest contribution over its full energy range is that of the 10 μm exit slit. The term due to the slope errors on the grating is smaller than that of the specified exit slit contribution over the full energy range of the gratings. The instrument was not designed for ultra-high photon energy resolution. Nevertheless, as shown in the figure, the monochromator will achieve a “resolving power” [11] better than 10^4 over its full scanning range with the MEG and the HEG.

Polarized flux

The beamline flux was calculated based on the flux emitted by insertion device, corrected for the bandwidth of the 10 μm slit, the reflectivity of all optical components, and the calculated grating efficiencies. The circular polarized flux emitted by the insertion device was calculated using SPECTRA [12]. The reflectivities of all optical components were obtained using the SRCalc code [13] assuming an RMS surface roughness of 0.2 nm. The gratings were assumed to be blazed and their efficiencies were calculated using the differential formalism of the exact electromagnetic theory [2]. We included an RMS surface roughness of 0.8 nm in the grating efficiency calculations.

The expected circularly polarized flux at the upstream experimental station for each of the three gratings is shown in Fig. 16b. With the LEG and the 10 μm exit slit (“resolving power” better than 4000) we expect a flux higher than 3×10^{13} photons/sec at the sample. The flux to be delivered by the MEG is higher than 7×10^{12} photons/s up to 1.5 keV. The use of the HEG will improve the “resolving power” to over 10^4 but will reduce the flux to 10^{12} photons/s up to 1.5 keV. The flux at the downstream experimental endstation will be reduced by approximately 1/2 due to the two additional mirror reflections.

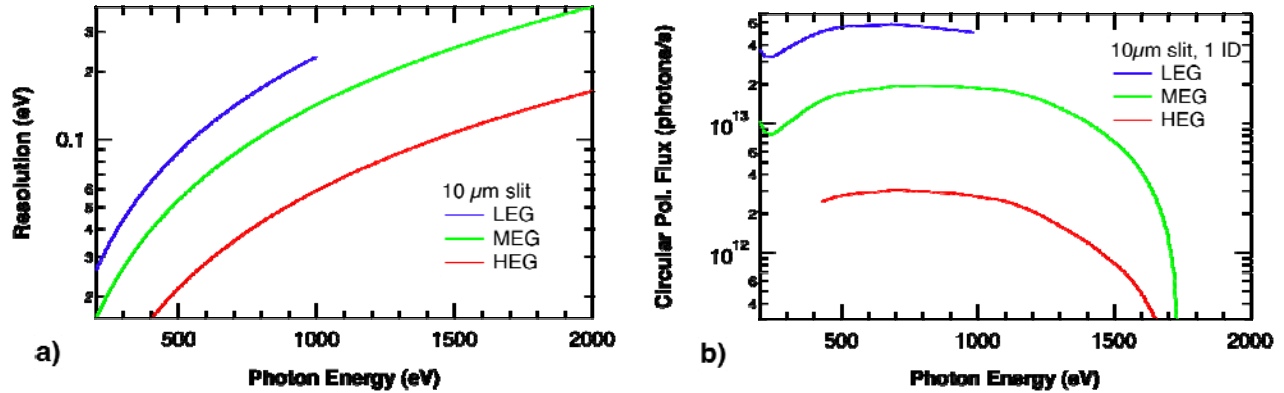


Figure 16. a) Expected resolution and b) expected flux at the upstream experimental endstation.

Other components at the beamline design also require our attention:

White beam apertures

First after the ratchet wall we find the water-cooled white beam apertures. These apertures will have the function to define the beam shape on the first optics and consequently reduce the heat load on the first optic element of each of the branches. The front end aperture will need to be able to remove in the worst case scenario of about 10 kW produced by the undulator with power densities up to 35 kW/mrad^2 . A diagnostic chamber should be located directly downstream of this element.

FEA analysis of the M1 Mirror

Finite element analysis has been conducted on a generic M1 internally water cooled mirror to ensure that the effects of the heat load on that element caused by the high power photon beams delivered by the insertion devices does not jeopardize the desired performance, such as high coherent photon flux in the coherent branch, and high photon flux combined with high energy resolution in the polarization branch.

Originally the first FEA results for this beamline were done with considering 2×2 meters long EPU45 in the worst case scenario, when horizontal polarized energy at 185 eV is emitted, see report in additional information APPENDIX. That study concluded that internally water-cooling on M1 mirrors is sufficient to achieve the state of the art performance of the beamline optics. Since that report the beamline layout has gone through some modifications. The change in the period length of the IDs from 45 to 49 mm only reinforces the considerations of the report. Nevertheless we have performed new FEA analysis varying the sizes and number of cooling channels in the mirror as well as its width and thickness. These new results are even more encouraging and we are very optimistic regarding the heat dissipation and future performance of the M1 beamline mirrors. Following we show some of the most recent FEA reported analysis. The results show the performance of an internally water-cooled mirror with 11 channels and 100 mm height considering the initial conditions of total power absorbed of 1.634 kW and a power distribution of 0.86 kW/urad^2 .

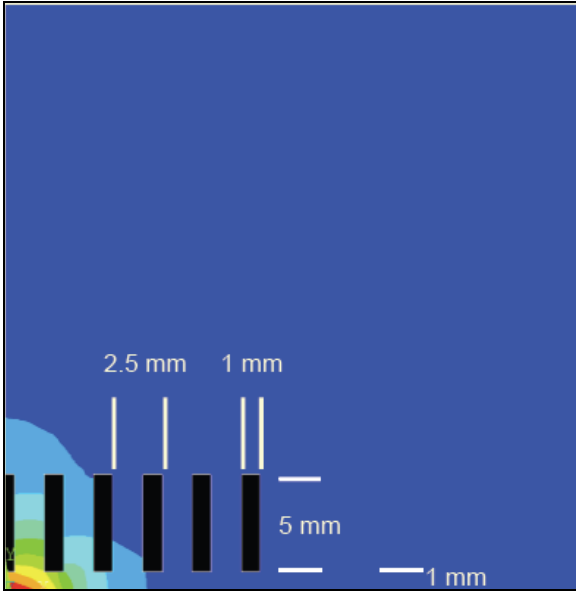


Figure 17. Partial view of a transverse section across the longest direction of the internal arrangement of the cooling channels in a 100mm x 100mm x 500mm internally water-cooled mirror with 11 channels along the beam direction (500 mm). The figure also shows that heat distribution is confined to a small region where the beam hits the mirror. (Simulations courtesy V. Ravindranath, figure courtesy R. Reininger NSLS-II)

The results of these simulations are very encouraging, because they show, see figure 18, that in the region of the central cone (≈ 200 mm) the induced PV slope error of such a mirror is less than $1 \mu\text{rad}$ along the meridional direction. Furthermore, the effect of this deformation can be corrected in the CB with the bendable M3-A mirror [2]. The effects of the heat load on the M2 monochromator mirrors has been described [2]... The most important result from that study is that the deformations on this mirror can be compensated by refocusing the monochromator.

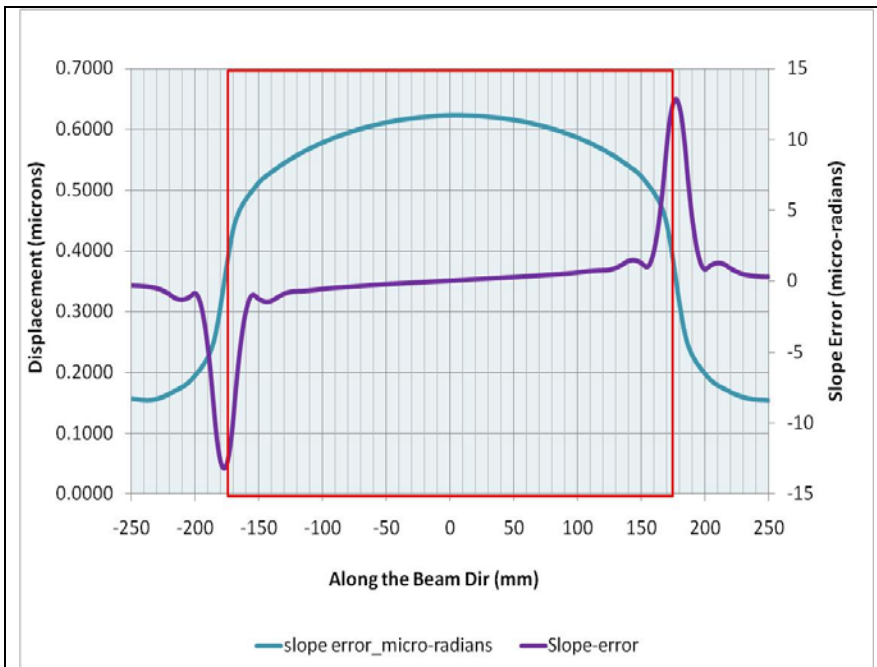


Figure 18 FEA analysis of an internally water cooled mirror with 11 channels. Inside the red box, that identifies the size of the mirror, the deformation along the surface (light blue) is less than 300 m, meanwhile the slope error (dark blue) is $>$ than 5 rad. Figures and simulations and figure courtesy V.Ravindranath (NSLS-II)

2.7 X-ray Tracing

Preliminary X-ray tracing was performed at the standard configuration for the CSX beamline. . Because of the soft x-ray nature of the radiation that this beamline will be working with, it is not expected to have complications in the X-ray tracing specific for the soft x-ray beamline optical layout. Once the optical design has achieved the mark of 90% .and the approval of the review we will initiate the beamline x-ray tracing

3 END STATION INSTRUMENTATION

Two end stations are planned, one dedicated to soft x-ray diffraction and imaging for the Coherent branch, and one optimized for resonant scattering dedicated to the fast-switching Polarization branch. But these will not be the only experiments at this beamline; the flexibility of the optical design allows two roll-up ports fulfilling the conditions of beam requirements established by the BAT. The diffraction and scattering end stations are being funded through capital funds from the Condensed Matter Physics and Materials Science (CMPMS) Department and the NSLS Department, respectively. It is expected that both end stations will be commissioned and operational at NSLS and kept state-of-the-art until being transitioned to NSLS-II. The instruments that will serve in the two open roll-up ports have not yet been determined.

Soft X-ray Diffraction and Imaging Vacuum Chamber for the Coherent Branch

This end station will consist of a 6-circle, in-vacuum diffractometer equipped with x-ray focusing optics to carry out combined diffraction and imaging experiments. The end station will feature the appropriate degrees of freedom to carry out full grazing incidence diffraction experiments with large in-plane components to the momentum transfer, and zone plate focusing optics to perform imaging experiments with spatial resolutions down to 40 nm at NSLS-II. Sample cooling will be provided down to 5K and the application of a magnetic field is being actively pursued. This station will be unique, in that it will be able to perform simultaneous grazing incidence diffraction and circular and linear dichroism and diffraction contrast imaging experiments.

Table 3. Diffraction and Imaging chamber major components

Diffraction chamber	Comments
In-vacuum diffractometer	6 circles in-vacuum diffractometer
Suite of detectors	
Suite of pinholes	
Zone plate	
Sample cooling	Control and monitor
Sample transfer system	
Polarization analysis	

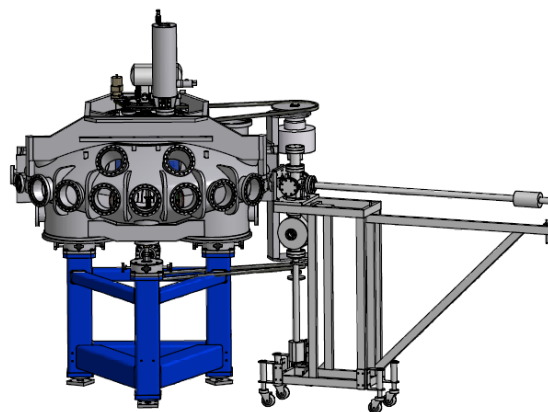
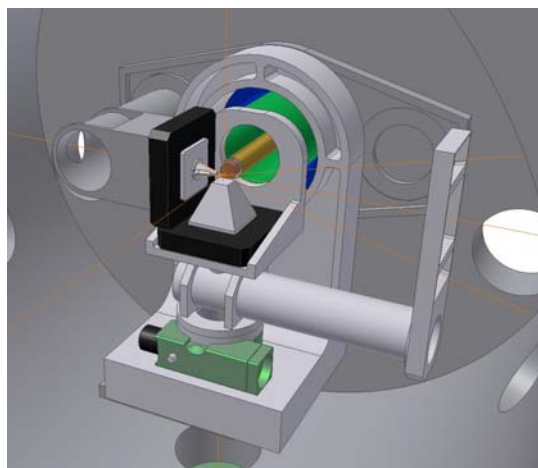


Figure 18: left, detail of in-vacuum diffractometer and sample stage in diffraction/coherent imaging vacuum chamber, right, scattering chamber with sample transfer for polarization branch.

Soft X-ray Resonant Scattering/Spectroscopy with a 1-Tesla Magnet for the Fast Switching Branch

The proposed state-of-the-art endstation will be an advanced upgrade of the NSLS X13A endstation and will have the following new features requested by the user community: (a) a new magnet, based on high temperature superconductor technology, to provide a magnetic field available at the sample position of ~ 1 T; (b) a more flexible scattering geometry (with magnetic field), permitting both longitudinal and transverse magneto-optical scattering geometries; (c) extension of the low-temperature limit down to ~ 10 K; (d) full coverage of scattering angle; (e) a suite of detectors to cover the full spectral range, with large dynamic range; and (f) a sample transfer system to allow a fast sample interchange.

Table 4. Scattering chamber major components

Scattering Chamber	Comments
Superconducting magnet	1 Tesla field, along the beam direction and along the perpendicular plane
In-vacuum diffractometer	Sample stage (x, y, z) and theta, detector arm -2θ
Suite of detectors	Electron yield, photon yield, and provision for water cooled detectors and area detectors
Sample cooling (< 20 k)	Control and monitor
Sample transfer system	With parking for precooled samples
Azimuth rotation on sample	360 degrees rotation
Polarization analysis	

4 SPECIAL BEAMLINE REQUIREMENTS

This windowless soft x-ray beamline working under UHV conditions is not expected to have special requirements that are currently not common at synchrotron facilities. Nevertheless in this section it is intended to list, the requirements for the beamline regarding normal operation or for special operations.

Time request for ultrafast experiments

Timing experiments, particularly pump-probe measurements at ultrafast (picosecond-scale) timescales, are an important aspect of experiments conducted at soft x-ray beamlines. For these experiments to be performed at the CSX beamline required non-standard photon timing patterns, bunch lengths and for the experiment control signals provided by the accelerator systems.

NSLS-II current plans is to operate at a master frequency of 500 MHz with a “standard” mode of operation with a near-uniform fill pattern, this will create difficulties for pump probe type ultrafast timing experiments. We propose to have additional machine operation modes with timing patterns a) with ~ 5 times larger bunch-to-bunch separation of at least 10ns, and b) a mode where a “superbunch” or “camshaft bunch” is well separated in time from the bunch train.

Ultrafast experiments will require the delivery by the “machine signal controls group” the signals that will allow: monitoring the operation mode or fill distribution pattern, the timing signal with a resolution of 400ps and a jitter of less than 5 ps. Also important for these experiments are the signals that allow monitoring of the deleterious effect of static *rf* cavities will introduce in the bunch length, and the relative phase relative to the master frequency, For more information we refer the reader to the APPENDIX 4.

Data storage and data processing for coherent imaging techniques

The following table provides an estimate for the need of the data storage and processing for a technique such as coherent imaging based on the detection of the diffraction pattern with a state-of-the-art CCD detector. The estimations are based on the calculated performance of the coherent scattering branch for more information about the data collection and processing estimates we refer the reader to the APPENDIX 4.

Table 5 System Data Requirements

Detector Size	2048 x 2048 pixels (larger in the future)
Detector Frame Rate	500 Hz
Peak data throughput	~ 4 GigaBytes/second
Average data throughput	~ 1 GigaByte/hour
Total daily storage capacity	10-20 GigaBytes
Total On-Sight storage	10 TeraBytes
Network Bandwidth	Gigabit ethernet
System control PC (motor control and data reduction)	Dual Quad-core CPU

These estimates do not consider the use of the simultaneous use of the two branches, what could easily add a factor 2 to the presented estimates.

With the demands of the new sources of the type of Free Electron Lasers, it is a very interesting time to observe and participate in the development of array detectors dedicated to diffraction imaging purposes. We anticipate that especially the coherent branch as the development advances the detection scheme in that branch will

be modified to incorporate one of these new detectors if this will improve the data acquisition time. In this case it is difficult to foresee the needs that the beamline will have if each of the branches will engage simultaneously in the utilization of one of these detectors. It is our intention to closely follow up the improvements in the detector technology, not only in the area of CCD detectors but also in any new type of 2D area detector that could serve the purposes of the beamline. Other areas that need follow up is in the data collection schemes as well as well as in the data processing, with the goal to achieve a best in class state-of-the-art data collection system.

Other requirements for this beamline are listed below,

- It is desirable for the operation of the beamline to have exhaust lines for the mechanical pumps to reduce the fumes and odors in the experimental floor. These should be flexible and have the capacity to handle 5 end stations simultaneously.
- Special exhaust lines with HEPA filters for experiments using “contaminant” gases that are not possible to use the normal exhaust lines. Using in the chambers elements such as chlorine and fluorine or in experiments dedicated to the observation of nanoparticles in suspension, not engineered to the substrate. With the capacity to handle two end stations at a time.
- Cabins of transparent material to cover and protect the beamline optical components from dust and accidental “bumps”. These cabins, located downstream of the First optic enclosure, downstream of the monochromator will not required to be radiation safe. Their function is to protect the equipment from dust, accidental bumps, and to minimize, if possible, temperature fluctuations caused by the close location of the beamline to the experimental floor access door.
- Soundproof experimental cabin. Until the optics design has not been finalize, and because of the limited space on the experimental floor, the existence, number, size or location on the experimental floor has not been defined.

There is also the need to keep the racks with electronics as far as possible from the beamlines to avoid vibrations, electrical noise and/or heat load transfer to the equipment.

- And regarding the utilities: the beamline will require to have: helium gas recovery, liquid nitrogen, boiled off Nitrogen gas for venting beamline components, compressed air for valves.
- Regarding the power it is very important to consider that this beamline has the capability to operate two branches at the same time, the clean power for detectors as well as the conventional power has to be sufficient to operate simulataneously two branches with their respective endstations.
- UPS up to 12 hours only for computers and area detectors at the beamline

5 REFERENCES

- [1] F. Riemer and R. Torge, Nucl. Instr. Methods 208, 313(1983).
- [2] R. Reininger, K. Kriesel, S. Hulbert, C. Sanchez-Hanke, and D. Arena, Rev. Sci. Instrum. 79, 033108 (2008).
- [3] M. Neviere, P. Vincent, and R. Petit, Nouv. Rev. Optique 5, 65 (1974).
- [4] T. Tanaka and H. Kitamura, Journal of Synchrotron Radiation 8, 1221 (2001).
- [5].M. Itou, T. Harada, and T. Kita, Appl. Opt., 28, 146 (1989)
- [6] R. Reininger and ARB de Castro, Nucl. Instrum. Methods A, 538, 760 (2005)
- [7] R. Reininger, K. Kriesel, S.L. Hulbert, C. Sánchez-Hanke, and D.A. Arena, Rev. Sci Instrum.79, 033108 (2008)
- [8] i.e., higher demagnification as seen in Table 1.
- [9] C. Welnak, G.J. Chen, and F. Cerrina, Nucl. Instr. Methods A, 347, 344, 1994
- [10]P. Elleaume, Undulator radiation, in Undulators, wigglers and their applications, H. Onuki and P. Elleaume, Editors. 2003, Taylor & Francis: London.
- [11] We use “Resolving Power” to indicate that the contribution of the slit is also taken into account
- [12] T. Tanaka and H. Kitamura. Spectra - a synchrotron radiation calculation code. J. Synchrotron Radiation, 8, 1221 (2001)
- [13] R. Reininger, SRCalc, 2001-2009

APPENDIX 1: SCHEDULE

The CSX beamline main critical characteristic the total number of optics needed in this design. The CSX beamline team is aware of the difficulties and risk that this is for the construction of the beamline. Following it is a list of milestones for the CSX beamline from now up to delivery of the first beam in April 2015 and it should not surprise anybody that these milestones are centered in the on time acquisition of the optics for the beamline. We understand that other items should not be neglected and they will appear also in this list.

- FY10 Finalize FEA and wavefront analysis for both branches, to confirm the performance and finalize 100% the optical design.
- Preliminary Design review: will contain all the calculations confirming the performance and feasibility of the optical layout.
 - Beamline optics final specification Specification of the CSX beamline optics will allow to start an early procurement process for the optics that are currently available in the market. With 9 optical components between monochromators and mirror optics, the CSX beamline team recognize this as one of the critical aspects of the CSX beamline.
 - Work closely with the ASD to specify the CSX beamline magnets: a) two times 2m long EPU49, b) phasing magnet and c) canting magnets. In all three magnetic systems the CSX team will strongly need to interact with the magnet designers and the head of the ID group in the ASD to specify all three types of magnets.
 - Specification and detail design of rest of the beamline components with special focus on beam diagnostic chambers, beam characterization chambers, apertures/exit slits/pinholes and chopper chamber.
 - Specification of first experiments to be performed at the beamline:
 - In the following year FY10 the beamline will strongly engage in possible upgrades of the two endstations, and specify the experiments for the roll-up ports.
 - Moment to start with new hiring for the CSX beamline
- FY11 Final design report
- Progress with procurement process for the major/critical optical components with long lead time because of not enough vendors in the market. This is going to be very critical for many of the CSX beamline.
 - Final design report : in this year we should finalize the design of all the beamline components optics chambers, diagnostics chambers and chambers for the roll-up ports, and other beamline components specially the ones that need to be engineered and build in-House.
 - Start the procurement of chambers for the different optical components.
- FY12 Final design report
- Start of the process of test of the optics specifications, assembly of the optical components and storage in LOB laboratories of first optical components start arriving. Keep the optics in save place until access to the experimental floor is granted.
 - Construction of the First Optic enclosure
 - Start of preliminary surveyors activities to precisely locate the beamline components on the experimental floor. And as soon as possible start placing optical components at the beamline.
- FY13 Beamline assembly.
- In this period the beamline personal will be working closely together with surveyors, utilities groups, and engineers to test the different components and safety systems before x-rays are available. Searching for beamline readiness to take beam.

- FY14 Start of one year of beamline commissioning time.
This will strongly depend on the availability of usable beam in the facility, presence of the IDs in the straight section and the close collaboration with the ASD.
- FY15 Start of expert user access to the beamline after one year of commissioning time

APPENDIX 2: ADDITIONAL INFORMATION

Previous Facility reports

NSLS-II Conceptual design report, chapter_11 Experimental Facilities pp 11-93 to 11-100
http://www.bnl.gov/nsls2/project/CDR/Ch_11_Experimental_Facilities.pdf

NSLS-II preliminary design report, part 2, "coherent soft x-ray beamline, pp 4-1 to 4_15, and all APPENDIXES pp 16-75,
http://www.bnl.gov/nsls2/project/PDR/2-ExFac_Ch_004_CSX.PDF]

The pdf files are attached to this document.

Timing requirements for ultrafast experiments (by D. Arena)

Timing experiments, particularly pump-probe measurements at ultrafast (picosecond-scale) timescales, are an increasingly important aspect of experiments conducted at soft x-ray beam lines. We present here the requirements for the CSX beamline at NSLS-II for both the photon timing patterns and bunch lengths, and the control signals necessary to mitigate potential deleterious effects and enable user timing experiments.

NSLS-II will operate at a master frequency of 500 MHz. The timing patterns are yet to be determined, but initial discussions indicate that the "standard" mode of operation will strive for a near-uniform fill pattern. This creates difficulties for ultrafast timing experiments employing a pump-probe architecture (where the x-ray pulses are the probe) as the bunch-to-bunch separation will be only 2 ns. For pump-probe experiments, the system must return to the initial state after an excitation (pump event), and characteristic damping times for many systems are longer than 2 ns. Thus the CSX beam line requires that some operating modes incorporate longer times between bunches. The two candidate timing patterns include (1) a bunch-to-bunch separation of at least 10 ns, and (2) a separate mode where a "superbunch" or "camshaft bunch" is well separated in time from the bunch train with 2 ns spacing.

Another aspect of the NSLS-II that affects ultrafast timing experiments is the passive *rf* cavities that may be installed to stretch the electron bunches longitudinally and hence reduce the electron emittance. This has deleterious effects for ultrafast timing experiments. First, the bunch length can increase considerably (close to a factor of two). This immediately reduces the time resolution of experiments as the minimum point-to-point resolution is determined by the photon bunch length. Second, the passive *rf* cavities introduce a phase delay, relative to the master *rf* frequency, as a function of position along the electron bunch train. After saturation, the difference in phase may be as large as 20°. The effect saturates, so that after a number of bunches after the ion clearing gaps, the change in phase remains constant. The CSX beam line requires an appropriate signal delivered to the beam line, indicating the position in time, or, equivalently, location along the bunch train where the change in the phase of the photon bunches is zero.

With regard to other control signals, the CSX beam line requires a timing signal based on the VME-EVR-230RF electronics or equivalent (or even an improved version of the system). This system can deliver a timing resolution of 400 ps and a jitter of less than 5 ps. This should be considered the minimally acceptable timing resolution. For comparison, the Advanced Photon Source delivers a timing signal with 18.5 ps resolution. The CSX project believes an improved specification is highly desirable, at the level of 5 ps or better. One possible option is to request that the controls group implement a local electronic delay line at the beam line (perhaps by use of the 10 Gb/s programmable digital delay line, model PDDL10 from Gigabaudics, Inc., or equivalent).

In addition to these signals, the CSX beam line requires a real-time distribution of the fill pattern to accommodate the selection of appropriate timing windows. Finally, blanking signals indicating fill events will also be necessary.

Estimates for data storage and data processing (by D. Shapiro)

If we assume that the coherent soft x-ray beamline delivers 10^{13} coherent photons per second and that the optical system is reasonably similar to current state-of-the-art facilities (i.e. provides the same spot size at the sample but with reduced divergence) then we can expect an increase of 10^4 in coherent flux density at the sample over those same facilities. As an example, diffraction microscopes at the ALS can record data to 10 nm resolution with exposure times of a few hundred seconds. Since the cross-section for coherent scattering goes with r^{-4} , NSLS-II should expect to produce diffraction data out to 1 nm resolution in a comparable time. This would be the ultimate experiment and not available from day one. A more conservative estimate is to expect imaging of 2 micron objects at 5 nm resolution. Using typical sampling geometries for data collection this requires a detector with 2000x2000 pixels. Imaging the same particle at 1 nm resolution requires AT LEAST 4000x4000 pixels or 10Kx10K using typical sampling rates.

Current state-of-the-art CCD detectors can produce 2×10^7 single precision data points per second. It is not unreasonable to assume that in 5 years time this will reach 2×10^9 data points per second. Thus, high throughput diffraction imaging systems will need a peak data bandwidth of 4 GigaBytes/second. This bandwidth can currently be provided by the PCI express architecture though a single 12 hour shift of data collection at this bandwidth would produce 173 TeraBytes of data! The solution to this problem is rapid on-sight data reduction since much of the recorded x-ray diffraction data is redundant and only needed to improve image statistics. Furthermore, the total data production rate will be limited by the practical problem of sample exchange. A conservative estimate would require 3 hours time for a completed tomographic dataset. Therefore, after data reduction, the total stored data per day would approach 10 GigaBytes. The data reduction itself could be performed by a reasonably fast multi-CPU desktop computer.

Efficient imaging requires near-instantaneous feedback to the scientist. One of the capabilities provided by high-brilliance light sources is high-speed imaging at high-resolution. For the case of imaging from diffraction data this requires not only a high coherent photon flux but also significant computational power. Each reconstruction requires thousands of Fourier transforms and each Fourier transform is a near TeraFLOP calculation for the three-dimensional case. This level of computational throughput can only be achieved when thousands of processing cores work in parallel. This can be provided by a multi-million dollar CPU cluster or a small cluster of massively parallel Graphical Processing Units (GPUs). A graphics card, such as the nVidia C1060 card, can provide the needed compute speed in a low-cost and low-power consuming package. A four-card compute node has a peak performance of 4 TeraFLOPS and could provide three-dimensional reconstructions in an hour. Similarly, it can provide instantaneous feedback to the microscope user by producing two dimensional reconstructions in just a few seconds.

System Data Requirements

Detector Size	2048 x 2048 pixels (bigger later)
Detector Frame Rate	500 Hz
Peak data throughput	~ 4 GigaBytes/second
Average data throughput	~ 1 GigaByte/hour
Total daily storage capacity	10-20 GigaBytes
Total On-Sight storage	10 TeraBytes
Network Bandwidth	Gigabit ethernet
System control PC (motor control and data reduction)	Dual Quad-core CPU